Severe corrosion of carbon steel in oil field produced water can be linked to methanogenic archaea containing a special type of [NiFe] hydrogenase.

Sven Lahme,[a]# Jaspreet Mand,[a] John Longwell,[a] Ramsey Smith,[a] and Dennis Enning[a]#

[a]ExxonMobil Upstream Research Company, Spring, Texas, USA

Running Head: Methanogenic MIC mechanism

#Address correspondence to Sven Lahme, sven.a.lahme@exxonmobil.com and Dennis Enning, dennis.r.enning@exxonmobil.com

ABSTRACT

Methanogenic archaea have long been implicated in microbially influenced corrosion (MIC) of oil and gas infrastructure, yet a first understanding of the underlying molecular mechanisms has only recently emerged. We surveyed pipeline-associated microbiomes from geographically distinct oil field facilities and found methanogens to account for 0.2 – 9.3% of the sequenced communities. Neither the type nor the abundance of the detected methanogens correlated to the perceived severity of MIC in these pipelines. Using fluids from one pipeline, MIC was reproduced in the laboratory, both under stagnant conditions and in customized corrosion reactors simulating pipeline flow. High corrosion rates (up to 2.43 mm Fe^0 yr^{-1}) with macroscopic, localized corrosion features were attributed to lithotrophic, mesophilic microbial activity. Other laboratory tests with the same waters yielded negligible corrosion rates (< 0.08 mm Fe^0 yr^{-1}). Recently a novel [NiFe] hydrogenase, from *Methanococcus maripaludis* strain OS7, was demonstrated to accelerate corrosion. We developed a specific qPCR assay and detected the gene encoding the large subunit of this hydrogenase (labelled *micH*) in corrosive (> 0.15 mm Fe^0 yr^{-1}) biofilms. The *micH* gene on the other hand was absent in non-corrosive biofilms despite an abundance of methanogens. Reconstruction of a nearly complete *Methanococcus maripaludis* genome from a highly corrosive mixed biofilm revealed *micH* and associated genes in near-identical genetic configuration as strain OS7, thereby supporting our hypothesis that the encoded molecular mechanism contributed to corrosion. Lastly, the proposed MIC biomarker was detected in multiple oil fields, indicating a geographically widespread involvement of this [NiFe] hydrogenase in MIC.

IMPORTANCE

Microorganisms can deteriorate built environments, which is particularly problematic in the case of pipelines transporting hydrocarbons to industrial end users. MIC is notoriously difficult

to detect and monitor and as a consequence, is a particularly difficult corrosion mechanism to manage. Despite the advent of molecular tools and improved microbial monitoring strategies for oil and gas operations, specific underlying MIC mechanisms in pipelines remain largely enigmatic. Emerging mechanistic understanding of methanogenic MIC derived from pure culture work allowed us to develop a qPCR assay that distinguishes technically problematic from benign methanogens in a West African oil field. Detection of the same gene in geographically diverse samples from North America hints at the widespread applicability of this assay. The research presented here offers a step towards a mechanistic understanding of biocorrosion in oil fields and introduces a binary marker for (methanogenic) MIC that can find application in corrosion management programs in industrial settings.

INTRODUCTION

Microbially influenced corrosion (MIC) is problematic to oil field operations when it leads to extensive damage requiring the repair or replacement of infrastructure such as carbon steel pipelines. While some metal loss is expected and accounted for during the design of the infrastructure (e.g. 0.1 mm yr^{-1} for a pipeline designed with 3 mm corrosion allowance for 30 years design life), higher rates of corrosion, unless detected and mitigated in a timely manner, can necessitate costly repairs or replacements long before the design service life has been actualized.

The most common oil field corrosion mechanisms are linked to CO_2 and/or hydrogen sulfide (H_2S) which are present in oil-bearing formations and readily dissolve into the water that is associated with production fluids (termed produced water). The deleterious effects of these acid gases are managed through injection of corrosion inhibitors (CIs), typically film-forming surfactants that act as a diffusion barrier between steel and the aqueous corrosive environment (1, 2). Acid gas corrosion can be modeled *in silico* (3) or simulated in laboratory reactors (4) to

68 understand the rates of metal loss expected under specific field conditions (i.e. flow, temperature,
69 brine chemistry and partial pressure of acid gases). Furthermore, laboratory testing provides a
70 robust approach to ensure CI effectiveness (4, 5). Microbial corrosion, on the other hand, cannot
71 be adequately modeled and laboratory qualification of oil field biocides, applied to control MIC,
72 typically falls short at predicting product effectiveness in the field. As a consequence, field-based
73 detection and monitoring is particularly important for effective management of this corrosion
74 mechanism.

75 In environments devoid of oxygen, MIC has been linked to a variety of anaerobic
76 microorganisms ((6) and references therein); yet most attention has historically been given to the
77 sulfate-reducing bacteria (SRB) due to their well-documented ability to cause severe corrosion in
78 laboratory studies and their prevalence in production systems ((7) and references therein). SRB
79 impact metal integrity by producing hydrogen sulfide (H_2S) as a corrosive metabolic end-product
80 of sulfate reduction with (usually) organic electron donors. A small number of lithotrophic SRB
81 isolates have further been shown to severely accelerate corrosion of steel in laboratory tests by
82 utilizing cathodic electrons for their metabolism (8–10). It was proposed that outer membrane c-
83 type cytochromes enable the direct uptake of electrons from steel in one such isolate, *Desulfovibrio*
84 *ferrophilus* strain IS5 (11). In addition to SRB, also methanogenic archaea are increasingly viewed
85 as prime culprits in the corrosion of steel (12–19). Some methanogens have been shown to utilize
86 metallic iron (Fe^0) in carbon steel as the sole electron donor for methanogenesis (13, 14, 19, 20).
87 Electrochemical studies suggested a mediator-free direct electron uptake mechanism for one of
88 these Fe^0-utilizing isolates, *Methanobacterium*-like strain IM1 (21). The potential technical
89 relevance of this microorganism has been demonstrated in laboratory studies where strain IM1 was
90 grown in flow-through systems (22).

91 A deeper understanding of the underlying biochemical basis of Fe^0 utilization by
92 methanogenic archaea has recently been provided. By working with filtered spent culture medium
93 as well as hydrogenase-negative mutants of *Methanococcus maripaludis* strain MM901,
94 Deutzmann and colleagues demonstrated that free, steel-associated hydrogenases from this strain
95 catalyzed the production of hydrogen (H_2) from Fe^0 granules (23). Whether these hydrogenases
96 originated from partial lysis of the laboratory culture (e.g. in stationary phase) or were actively
97 excreted is currently unknown. Likewise, it is unclear whether this mechanism can produce
98 technically relevant MIC in laboratory or oil field settings. Tsurumaru and colleagues performed
99 comparative genomics on multiple strains of *Methanococcus maripaludis* and identified a 12 kb
100 genomic region (termed 'MIC island') that was unique to pure cultures of strain OS7, the only
101 strain of *M. maripaludis* that accelerated Fe^0 oxidation (corrosion) in their tests (24). This 'MIC
102 island' encoded for a novel type of [NiFe] hydrogenase along with an extracellular transport
103 system. It was postulated that the secreted [NiFe] hydrogenase would catalyze the reduction of H^+
104 to molecular hydrogen on iron surfaces, thereby accelerating the oxidation of the provided iron
105 granules.

106 These recent insights into the molecular mechanisms of MIC by methanogenic archaea
107 prompted us to investigate the role of methanogens in the corrosion of oil and gas infrastructure.
108 Since MIC is a biofilm-associated phenomenon (25), we began by surveying the archaeal
109 microbiomes of steel-associated solids from pipelines in North America, East Asia and West
110 Africa. We then performed a comprehensive study of MIC using produced waters from one of
111 these locations in controlled laboratory reactors that allowed for the growth of methanogenic
112 archaea. The extent of corrosion as well as associated microbial communities were investigated
113 under various enrichment conditions with natural oil field waters, as well as synthetic brines to

114 specifically enrich for lithotrophic microorganisms. Building on these laboratory tests, we gained
115 insights into the molecular mechanisms of MIC through shotgun DNA sequencing and
116 metagenomic analysis of a highly corrosive, lithotrophic biofilm grown under simulated pipeline
117 conditions. Lastly, we developed a novel qPCR assay for the detection of the abovementioned
118 [NiFe] hydrogenase and demonstrated the applicability of this proposed MIC biomarker assay in
119 industrial settings.

120 **RESULTS**

121 **Methanogenic archaeal communities on carbon steel pipeline walls**

122 Maintenance of oil field pipelines involves the periodic use of devices with blades or
123 brushes (termed 'pig', pipeline intervention gadget) to mechanically clean out rust, wax, scale and
124 biofilm (collectively termed 'pig debris'). This practice offers the opportunity to access steel-
125 associated microorganisms from pressurized hydrocarbon pipelines. We obtained pig debris from
126 nine different pipelines in seven geographically distinct oil field operations in North America, East
127 Asia and West Africa to survey the prevalence of methanogenic archaea (Fig. 1). Estimated 16S
128 rRNA gene abundances of $1.6 \cdot 10^7$ - $1.3 \cdot 10^{10}$ gene copies per g of pig debris suggested moderately
129 dense microbial colonization of pipe wall-associated solids. Archaeal sequences accounted for 0.2
130 – 21.6% of total reads, and most of the detected archaea were classified as members of
131 methanogenic archaeal families (0.2 – 9.3% of total reads). Members of the *Methanococcaceae*,
132 *Methanobacteriaceae*, and *Methanosarcinaceae* have been implicated in MIC through laboratory
133 investigations (13, 17, 19, 24). However, there was no apparent correlation between the types or
134 abundances of methanogens, and the perceived severity of MIC in the surveyed pipelines (Fig. 1).
135 For example, pipelines [A] – [C] had no indications of active internal corrosion (MIC or otherwise)

136 in recent in-line inspections (ILI, data not shown) despite the presence of microorganisms
137 affiliating with the abovementioned putatively corrosive archaeal families.

138 **Assessment of MIC under mesophilic and thermophilic conditions**

139 The detection of methanogenic archaea in all surveyed pipelines necessitated a more
140 nuanced understanding of their potential role in corrosion; a question that was approached through
141 laboratory cultivation. We hence obtained anoxic production fluids from a West African oil field
142 with a history of MIC (Fig. 1, pipelines [G] and [I]). Carbon steel infrastructure typically spans
143 broad temperature gradients within the same oil field due to hot production fluids from reservoirs
144 (often >> 60ºC) cooling as they pass through networks of pipelines, pressure vessels and piping.
145 Fluids from subsea pipeline [I] had an average temperature of 32ºC at the time of sampling. In the
146 laboratory, the sulfate-free (< 20 μM) produced water was transferred into glass bottles with
147 specially designed carbon steel coupon holders with rubber stoppers and an anoxic headspace of
148 N_2-CO_2. Bottles were incubated at 32°C and 60°C on rotary shakers (75 rpm) for 13 weeks; under
149 conditions that are most representative of process dead legs or idled pipelines (i.e. stagnant to very
150 low flow). Indeed, methanogenic biofilms developed on carbon steel surfaces exposed to the
151 sulfate-free produced water, as evidenced by accumulation of CH_4 in the test bottles (Fig. 2A) and
152 detection of high numbers of steel-attached methanogenic archaea through qPCR and 16S rRNA
153 gene sequencing (Fig. 2A and B). Methanogens accounted for 17.0 – 54.4% of the steel-attached
154 biofilms. Archaeal communities grown at 32°C showed high abundances of hydrogenotrophic (i.e.
155 lithotrophic) *Methanobacterium* spp. and *Methanocalculus* spp., with minor fractions of
156 *Methanococcus* spp. Incubation at higher temperatures (60°C) led to formation of biofilms with
157 prominent fractions of hydrogenotrophic *Methanothermobacter* spp. and, at lower prevalence, the
158 acetoclastic *Methanosaeta* spp. (Fig. 2B). Mesophilic bacterial communities (32°C) contained

159 high fractions of *Syntrophomonas* spp., *Kosmotoga* spp. and *Halomonas* spp. that might have
160 grown through fermentation of residual organic compounds in the produced water, thereby
161 producing acetate, CO_2 and H_2 (26–28). The majority of the biofilm community in bottles
162 incubated at 60°C consisted of mesophilic bacteria unlikely to grow at that temperature (Fig. 2C).
163 However, some thermophilic bacteria such as *Thermotoga*, *Fervibacterium* and *Caldithrix* were
164 detected and could have grown via a fermentative metabolism (29–31). Consistent with the lack
165 of sulfate in these natural oil field waters, we only detected minor fractions of SRB in steel-
166 attached biofilms (cumulatively < 0.6% per biofilm). The different incubation temperatures
167 resulted in markedly different metal damage (Fig. 2A). Microbial activity had negligible impact
168 on carbon steel at 60°C, with an increase in corrosion rates of approximately 40% compared to
169 sterile controls, but a low average corrosion rate of 0.02 ± 0.01 mm Fe^0 yr^{-1}. Mesophilic
170 microorganisms, on the other hand, accelerated corrosion by a factor of 12 and led to localized
171 damage with features as deep as 399 µm developing over 3 months (Fig. 2A and Fig. S1). The
172 National Association of Corrosion Engineers (NACE) categorizes corrosion rates of carbon steel
173 coupons > 0.13 mm Fe^0 yr^{-1} as *high* and > 0.25 mm Fe^0 yr^{-1} as *severe* (NACE SP0775-2013).
174 Interestingly, despite the profoundly different impacts on corrosion, biofilms grown at 32°C and
175 60°C contained similar numbers of active methanogens (Fig. 2A). This observation implied that
176 intrinsic properties of the mesophilic biofilm community rather than the overall cell number or
177 methanogenic activity were linked to the observed acceleration of corrosion kinetics.

178 **Identification of potential methanogenic corrosion mechanisms**

179 Tsurumaru and colleagues recently linked the accelerated oxidation of Fe^0 (i.e. corrosion)
180 in cultures of *M. maripaludis* strain OS7 to a novel [NiFe] hydrogenase (24). A protein sequence
181 comparison of the large subunit of this hydrogenase against the National Center for Biotechnology

182 Information's (NCBI) protein sequence database revealed that three sequenced members of the
183 *Methanobacteriales* contain similar proteins (90.7 to 93.5% protein sequence identity), while all
184 other deposited sequences showed ≤ 40% protein sequence identity (Table S1). The high degree
185 of protein sequence resemblance suggested functional similarity within this protein cluster and
186 prompted us to develop a specific qPCR assay. We developed a degenerated primer pair and
187 Taqman™ probe (Table 1) to detect and quantify the gene of the large subunit of the [NiFe]
188 hydrogenase (referred to here as *micH*) in strain OS7 and the three other methanogenic strains.
189 This assay allows for probing of mixed microbial biofilms for their ability to carry out a proven
190 microbial corrosion mechanism, i.e. the enzymatic catalysis of Fe^0 oxidation via an extracellular
191 hydrogenase. Intriguingly, we could detect $3.3 \cdot 10^2$ and $1.6 \cdot 10^3$ *micH* gene copies per cm^2 in
192 corrosive biofilms at 32°C while the *micH* gene was undetectable in non-corrosive biofilms grown
193 at 60°C (Fig. 2A). This raised the possibility that mesophilic, lithotrophic methanogens, likely of
194 the genera *Methanococcus* or *Methanobacterium,* had caused the observed high rates of corrosion.

195 **Enrichment of organotrophic and lithotrophic oil field communities**

196 We sought to reproduce our observations and collected a new batch of production fluids
197 from the same West African oil field. Traces of H_2S (approx. 100 ppm) measured in the gas phase
198 of the sample collection drums upon arrival in our laboratories indicated sulfate reduction, so we
199 amended the next tranche of corrosion bottle tests with sulfate to allow for the growth of SRB.
200 Again, highly corrosive mesophilic biofilms developed in these produced waters and putatively
201 corrosive *Methanococcus* spp., as well as *Methanocalculus* spp. were detected in large fractions
202 (Figs. 2D and 2E). Furthermore, these biofilms contained *micH* at even higher numbers than
203 previous cultures with $1.1 \cdot 10^5 – 7.4 \cdot 10^5$ gene copies per cm^2 (Fig. 2D).

204 The use of actual produced waters for laboratory studies offers the opportunity to closely
205 simulate oil field MIC in laboratory settings. However, it also complicates data interpretation,
206 since the presence of complex organic matter can allow for a multitude of fermentative and
207 oxidative metabolisms. We therefore dissected experimental conditions by working with defined
208 cultivation media which were modelled after the major ion composition of the original produced
209 water (+ sulfate). Organotrophic and lithotrophic enrichment cultures containing steel coupons
210 were set up with or without addition of organic acids (12.1 mM acetate and 1.6 mM propionate),
211 respectively. This reduced the number of potential biological transformations and, in the case of
212 tests without the organic acids, limited growth to those microorganisms capable of utilizing
213 metallic iron (Fe^0) as an electron donor. Transfer of produced water as inoculum (0.5% vol/vol)
214 into synthetic media reduced microbial corrosion rates to moderate rates (< 0.08 mm Fe^0 yr^{-1}) in
215 all but one of the bottle tests (Fig. 2D). Remarkably, this lithotrophic culture caused corrosion at
216 severe rates of 0.76 ± 0.15 mm Fe^0 yr^{-1}, with up to 370 µm deep corrosion features developing on
217 carbon steel coupons over 3 months (Fig. 2D and Fig. S2). All biofilms in the synthetic produced
218 water media were numerically dominated by sulfate-reducing bacteria, in particular *Desulfovibrio*
219 spp., *Desulfobulbus* spp. and *Desulfotignum* spp. (Fig. 2F). The distinguishing feature of the
220 severely corrosive lithotrophic biofilm, however, appeared to be the enrichment of a sub-
221 population of *Methanococcus* spp., and the detection of the special [NiFe] hydrogenase *micH*
222 (Figs. 2D and 2E).

223 **Corrosion under simulated pipeline condition**

224 The preceding bottle tests demonstrated the potential for severe MIC in stagnant water
225 bodies within infrastructure of the investigated oil field. However, the pipelines that transport
226 multi-phasic fluids (e.g. from offshore production wells) usually experience high flow and, as a

227 result, wall shear stresses, which greatly increase the rates of acid gas corrosion resulting from
228 CO_2 (32). Likewise, biofilm formation can be affected by the physical stresses imposed by flow
229 (33).

230 We therefore evaluated corrosion in customized test reactors (corrosion kettles) that allow
231 for close simulation of pipeline conditions by controlling shear stress, pH and acid gas composition
232 (Fig. 3A). First, a test with sterile synthetic produced water was performed to establish the baseline
233 corrosion from CO_2. These tests revealed that abiotic conditions alone could cause severe
234 corrosion of 0.34 ± 0.01 mm Fe^0 yr^{-1} (Fig. 3B and Fig. S3) under conditions that model pipelines
235 [G] and [I].

236 Still, inclusion of oil field microorganisms in these tests demonstrated the pronounced
237 biotic component of pipeline corrosion under the studied conditions; a second tests with actual
238 produced water increased averaged corrosion rates beyond the CO_2 baseline to 0.54 ± 0.14 mm
239 Fe^0 yr^{-1} (Fig. 3B), and resulted in irregular and localized pitting corrosion at extrapolated rates of
240 1.57 ± 0.61 mm yr^{-1} (Fig. 3B and Fig. S3). Operation of a third corrosion kettle with lithotrophic
241 produced water medium inoculated with a pre-enriched Fe^0-utilizing culture (asterisk in Fig. 2D)
242 resulted in even more aggressive metal damage. This culture catalyzed iron oxidation at rates of
243 1.62 ± 0.72 mm Fe^0 yr^{-1}, leading to macroscopic localized corrosion features with an extrapolated
244 growth rate of 5.24 ± 2.21 mm yr^{-1} over 7 weeks (Fig. 3C). Microbially catalyzed metal oxidation
245 at these rates, if left unmitigated, would profoundly challenge pipeline integrity.

246 High copy numbers of *micH* (> 10^6 copies per cm^2) and high relative fractions of 28% and
247 42% of *Methanococcus* spp. were detected in biofilms grown in corrosion kettles operated with
248 actual (organotrophic) and synthetic (lithotrophic) produced water, respectively (Fig. 3B and Fig.

249 S4). Other dominant microorganisms detected in corrosive biofilms in both reactors included
250 *Desulfovibrio* spp. (Fig. S4).

251 A fourth corrosion kettle was set up with synthetic produced water medium containing
252 organic acids and was inoculated with an organotrophic subculture from the West African oil field.
253 This test did not produce the previously observed high corrosion rates, despite formation of similar
254 biofilms as measured by 16S rRNA gene abundance (Fig. 3B). Corrosion of coupons underneath
255 these biofilms containing *Desulfovibrio*, *Desulfobulbus* and *Methanolobus* species (Fig. S4) was
256 considerably lower than the sterile control, at 0.073 ± 0.001 mm Fe^0 yr^{-1} and resulted in rather
257 uniform metal loss (Fig. 3B and Fig. S3). This may be an indication that the biofilm limited CO_2
258 corrosion by forming a passivating barrier, a phenomenon seen before in laboratory tests (Kip and
259 van Veen 2015 and references within). Notably, this 'protective' biofilm did not contain any
260 *Methanococcus* spp. or *Methanobacterium* spp. and tested negative for *micH* (Figs. 3B and S5).

261 **Genomes recovered from a severely corroded carbon steel coupon**

262 Shotgun metagenome analysis can be a useful tool to probe for blueprints of biochemical
263 reactions in mixed microbial communities. We wanted to further investigate the molecular
264 mechanisms of MIC seen in this study, and hence extracted and sequenced DNA of a biofilm that
265 was i) associated with severe corrosion, ii) contained high fractions of potential culprit organisms
266 such as *Methanococcus* spp. and *Desulfovibrio* spp. and iii) was grown under pipeline-like
267 conditions (see asterisk in Fig. 3B for selected sample).

268 We were able to obtain six near complete metagenome-assembled genomes (MAGs) from
269 this sample (Table 2). Taxonomic classification by protein marker analysis indicated that one of
270 the MAGs affiliated closest with *Methanococcus maripaludis*. The *micH* gene in *M. maripaludis*

271 strain OS7 is co-located on a 12 kb 'MIC island' with genes hypothesized to be essential for the
272 functioning and secretion of this hydrogenase (24). A sequence similarity search revealed that a
273 *micH* homolog was indeed present in one of the assembled contigs of the *M. maripaludis* MAG.
274 Furthermore, we discovered that the genetic arrangement of the 'MIC island' in this MAG and
275 strain OS7 was in fact identical (Fig. 4). Notably, the genetic island contained genes for both
276 subunits of the putative [NiFe] hydrogenase, as well as the twin-arginine translocation system for
277 secretion of the mature hydrogenase in strain OS7 (24). Protein sequence comparison further
278 confirmed a high resemblance (98.8 – 100% amino acid sequence identity) between both clusters
279 (Fig. 4).

280 Traditionally, SRB have been viewed as prime suspects of MIC (7). While all SRB can
281 produce corrosive H_2S under suitable organotrophic growth conditions, some specialized
282 lithotrophic SRB strains have recently received much attention as they can cause particularly
283 severe corrosion through a more direct mechanism (8, 9, 13). It had been proposed that these
284 organisms oxidize metal through direct electron uptake via outer-membrane c-type cytochromes
285 (OMCs, (13)), with recent evidence supporting this hypothesis in *D. ferrophilus* strain IS5 (11). In
286 this study, we obtained three near complete *Desulfovibrionaceae* genomes (Table 2). A reliable
287 taxonomic classification was possible for one genome, which was assigned to a strain of
288 *Desulfovibrio alaskensis*. However, despite presence of three near complete *Desulfovibrionaceae*
289 genomes, no evidence for a homologous OMC system to the one detected in strain IS5 was found
290 in this metagenomic dataset. This suggest that a direct electron uptake via extracellular c-type
291 cytochromes may not have contributed to MIC in our experiments.

292 The detection of *micH* in a metagenome-assembled genome from a highly corrosive
293 biofilm further strengthened the applicability of this gene as a potential marker for MIC. We

294 confirmed the presence of *micH* (up to $1.6 \cdot 10^6$ gene copies per g) in pig debris from the West
295 African oil field (pipelines [G] and [I] in Fig. 1). Intriguingly, we also detected $3.9 \cdot 10^3 – 2.8 \cdot 10^4$
296 *micH* gene copies per g in three geographically separated pipelines in North America (Fig. 1).

297 **DISCUSSION**

298 Methanogenic archaea are commonplace members of the oil field microbiome (16, 17, 34,
299 35). However, unlike SRB which produce corrosive sulfides as a metabolic product, methanogenic
300 archaea are not intrinsically corrosive (24, 36); they oxidize molecular hydrogen or a limited
301 spectrum of small organic compounds and produce chemically inert CH_4. We surveyed surface-
302 associated deposits from nine pipelines in seven geographically distinct oil field operations and
303 detected methanogenic archaea in all instances, despite vast differences in the perceived severity
304 of MIC (Fig. 1). For example, methanogens affiliated with the *Methanobacteriaceae*,
305 *Methanococcaceae* and *Methanosarcinaceae* were detected in steel-associated solids from
306 pipelines [A] - [C]. Members of these archaeal families have been implicated in MIC through
307 laboratory studies (13, 17, 19, 24), yet recent inspections of the pipelines [A] – [C] did not reveal
308 any indications of internal corrosion. Similarly, biofilms containing *Methanosaeta* spp.,
309 *Methanobacterium* spp., *Methanolobus* spp. and *Methanothermobacterium* spp. caused only
310 negligible corrosion (< 0.08 mm Fe^0 yr^{-1}) in laboratory reactors that simulated oil field conditions
311 (Figs. 2, 3 and S5). These data highlight that the mere presence of methanogenic biofilms on steel
312 does not entail corrosion.

313 Corrosion of metallic iron in the absence of oxygen can be depicted as follows:

314 $$Fe^0 \leftrightarrow Fe^{2+} + 2e^- \quad (1)$$

315 $$2e^- + 2H^+ \leftrightarrow H_2 \quad (2)$$

316 $$Fe^0 + 2H^+ \leftrightarrow Fe^{2+} + H_2 \quad (3)$$

317 Where the anodic oxidation of iron (reaction 1) is coupled to the cathodic reduction of a suitable
318 oxidant, in anoxic environments usually H^+ (reaction 2), so that the net reaction involves formation
319 of molecular H_2 (reaction 3). Reaction 2 is kinetically impeded and as a result the corrosion of
320 steel is slow in anoxic environment at near-neutral pH (9, 37, 38). However, corrosion in (slightly)
321 acidic oil field waters can be pronounced in the presence of weak acids, as loosely bound protons
322 from carbonic acid, organic acids or sulfide dramatically increase the availability of H^+ ions as
323 oxidants at the steel surface, particularly in high flow scenarios (39).

324 Historic models of MIC had postulated that the consumption of cathodic molecular
325 hydrogen by hydrogenotrophic microorganisms (incl. methanogens) would accelerate corrosion
326 (40–42). However, this view has been disputed based on kinetic and thermodynamic
327 considerations (8, 9, 43), as well as through copious experimental observations (8, 13, 14, 24, 36).
328 However, while the majority of tested hydrogenotrophic methanogenic archaea does not influence
329 steel oxidation to any significant extent, some strains have shown a pronounced impact on
330 corrosion kinetics in laboratory experiments (13, 14, 24, 36). Recently evidence has emerged that
331 some pure cultures of methanogenic archaea accelerate corrosion when they produce extracellular
332 hydrogenases that catalyze reaction 2 on steel surfaces (23, 24).

333 **Mesophilic methanogens in highly corrosive oil field biofilms contain a special MIC**
334 **hydrogenase**

335 In this study we reproduced oil field corrosion using fluids from an offshore production
336 site in West Africa. Formation of mesophilic biofilms considerably increased corrosion rates over
337 sterile controls, both in *de facto* stagnant bottle test, as well as in corrosion kettles simulating flow

338 and field-like partial pressures of CO_2 (Figs. 2 and 3). Technically highly relevant MIC rates (0.15
339 – 1.62 mm Fe^0 yr^{-1}) and severe pitting were observed in several of these bioreactors. By using
340 specially formulated synthetic produced water media we could further demonstrate that the
341 observed Fe^0 oxidation was in fact a lithotrophic process. Some hydrogenotrophic *Methanococcus*
342 spp. and *Methanobacterium* spp. have been shown to effectively utilize Fe^0 and were found in
343 substantial numbers (> $3.7 \cdot 10^5$ 16S rRNA gene copies per cm^2) in highly corrosive biofilms (Figs.
344 2 and 3; Fig. S5B). However, both genera were also present in nearly all other (non-corrosive)
345 biofilms, confirming that hydrogenotrophy itself does not accelerate corrosion kinetics.

346 Tsurumaru and colleagues recently discovered that only a few known strains of *M.*
347 *maripaludis* and *Methanobacterium* spp. encode for a unique hydrogenase that catalyzes the
348 reduction of H^+ to H_2 on Fe^0 granules and thereby considerably accelerates iron oxidation (24).
349 The apparent high conservation amongst proteins from members of *Methanococcaceae* and
350 *Methanobacteriaceae* allowed us to develop a specific qPCR assay targeting the gene of the large
351 subunit, *micH*, of this hydrogenase. This assay did in fact distinguish biofilms causing technically
352 relevant corrosion (> 0.13 mm Fe^0 yr^{-1}) from those that did not (< 0.08 mm Fe^0 yr^{-1}) in our
353 experiments with actual and synthetic produced waters (Fig. S5B, Figs. 2 and 3). *M. maripaludis*
354 strain OS7 harbors this unique hydrogenase (*micH*) on a 12 kbp long genetic island along with
355 several other genes assumed to be essential for a fully functional extracellular enzyme (24). We
356 were able to retrieve a near complete genome of a *Methanococcus maripaludis* strain that carried
357 *micH* in an identical genetic arrangement as strain OS7 (Fig. 4). This indicated that *micH* was
358 associated with a corrosive *Methanococcus maripaludis* strain in our laboratory tests. Indeed,
359 corrosive biofilms consistently contained both, methanococcal 16S rDNA and the *micH* gene (Fig.
360 S5B).

361 There was no linear correlation between the extent of corrosion and copy numbers of *micH*
362 (Fig. S5). High corrosion rates were observed on coupons containing as few as $3.3 \cdot 10^2$ gene copies
363 per cm^2 at the time of biofilm collection (Fig. 2A). It should be noted though that corrosion rates
364 were averaged from metal loss over the entire experimental period (e.g. 3 months), while
365 quantification and characterization of target genes in biofilms was only performed at test takedown
366 and hence only represents endpoint conditions. Methanogens precipitate siderite ($FeCO_3$) which
367 can passivate steel surfaces (18, 44) and could have buried initially corrosive methanogens in some
368 tests, possibly allowing for the degradation of 'forensic evidence'. This could explain low copy
369 numbers in some highly corrosive biofilms. More importantly though, we do not envision gene
370 copy numbers of *micH* to correlate with the final abundance of the actual enzyme that catalyzes
371 iron oxidation. Still, *micH* in biofilms served as a binary genetic marker for technically relevant
372 microbial corrosion in our tests with West African produced waters.

373 Methanogenic archaea constituted only a part, and in some instances a minor part of the
374 biofilm communities that developed under simulated oil field conditions. In addition to organic
375 compounds in the produced waters and the organotrophic synthetic produced water medium (e.g.
376 acetate and propionate), also small quantities of cathodic hydrogen from abiotic corrosion
377 according to reaction 3 will have served as a readily available electron donor, e.g. for sulfate-
378 reducing bacteria. It is tempting to speculate that enzymatically catalyzed H_2 formation from
379 extracellular hydrogenases could have fed additional electron donors into the biofilm community.
380 A potential role of electroactive H_2-forming microorganisms as 'ecosystem engineers' has been
381 proposed elsewhere (45).

382 **The role of sulfate-reducing bacteria in corrosion**

383 The importance of sulfate-reducing bacteria in microbial corrosion has long been
384 established ((7) and references therein) and the underlying mechanisms as well as their regulation
385 are still an active area of research (11, 46–48). While we cannot exclude contribution of SRB to
386 corrosion, we inferred that they had likely played a minor role in our experiments. Firstly,
387 *Desulfovibrio sp.* were found in high abundances in all biofilms under sulfate-reducing conditions,
388 but high or severe corrosion only occurred in the presence of *micH*-positive methanogens (Figs.
389 2D and 3B; Fig. S5). Secondly, high microbial corrosion rates were also observed in sulfate-free
390 produced water (Fig. 2A). Thirdly, only few lithotrophic SRB isolates have been demonstrated to
391 cause corrosion to an extent similar to what was observed in this study (7, 8); the extracellular
392 multiheme c-type cytochromes that have been linked to direct electron uptake in those corrosive
393 strains (11) were absent in the metagenomic dataset. The low to moderate corrosion rates in the
394 absence of *micH*-positive *Methanococcus* spp. agree with corrosion rates documented for
395 sulfidogenic cultures of *D. alaskensis* ($\leq$ 0.1 mm Fe^0 yr^{-1}; (22, 48, 49)). We cannot, however,
396 exclude that hitherto unknown enzymatic mechanisms may have affected corrosion in our
397 experiments.

398 **Proposed use of *micH* as a genetic marker for methanogenic MIC**

399 Microbial corrosion of oil field infrastructure is difficult to detect and monitor, in large part
400 because the responsible microorganisms and underlying mechanisms remain enigmatic (50). For
401 example, the mere presence of large numbers of methanogenic archaea in pipeline-associated
402 debris or laboratory-grown biofilms proved to be a poor indicator of MIC in this study (Fig. 1 and
403 Fig. S5). A deeper mechanistic understanding of MIC in methanogens and other environmental
404 microorganisms offers a route to a more granular analysis and interpretation of microbiological
405 monitoring data in oil fields and other industrial settings. Enzymatic acceleration of corrosion via

406 hydrogenases is one such potentially relevant corrosion mechanism. This was recently evidenced
407 through careful experimentation with pure cultures of methanogenic archaea (24) and
408 demonstrated in this study with mixed microbial communities in bioreactors simulating oil field
409 corrosion. We designed an assay to quantify the gene encoding for an extracellular hydrogenase
410 (*micH*) in methanogens and demonstrated its ability to serve as a binary marker for MIC in
411 experiments with oil field cultures grown under stagnant and pipeline flow-simulating conditions
412 (Fig. S5B). The proposed MIC biomarker was detected in high concentrations (up to $1.6 \cdot 10^6$ gene
413 copies per g) in pipeline-associated solids from a West African oil field with a history of MIC
414 (pipeline [I] in Fig. 1). Interestingly, we also detected *micH* in similar solids from pipelines on the
415 West Coast and Gulf Coast of the United States (Fig. 1). The genetic island carrying this gene was
416 first detected in *M. maripaludis* strain OS7, which originated from an underground oil storage tank
417 in Japan and was further detected in the genome of *Methanobacterium congolense* Buetzberg by
418 the same group (24). Strain Buetzberg was originally isolated from a biogas plant in Germany (51).
419 The fact that we were able to reconstruct a near identical 'MIC island' from a West African oil
420 field strain of *M. maripaludis* (Fig. 4) suggests an extremely high level of conservation of the 'MIC
421 island' and presence of these corrosive methanogens in industrial facilities across four continents.
422 Future work may focus on developing a better understanding for the quantitative interpretation of
423 *micH* in solid and liquid samples to enable early detection and mitigation of severe cases of
424 microbially influenced corrosion in industrial settings.

425 **MATERIALS AND METHODS**

426 **Collection of solid samples (pig debris) from pipelines**

427 Solids from nine carbon steel pipelines were collected between July 2014 and June 2017
428 to study the microbiomes within hydrocarbon-transporting infrastructure. Subsea pipelines [G] and

429 [I] transport fluids from one oil field offshore Nigeria. This field produces oil and sweet natural
430 gas (i.e. no H_2S). Subsea pipelines [C] and [H] transport fluids from an offshore oil field on the
431 U.S. West Coast. The other five pipelines each carry fluids from separate oil and gas fields on the
432 U.S. West Coast [E], Midwest [F] and Gulf Coast [B, D], as well as from East Asia (A). Samples
433 were collected following the (internal) mechanical cleaning of these pipelines with maintenance
434 pigs that remove and push out surface-associated and settled debris. These solid samples (collected
435 in the pig trap) were carefully transferred into sterile containers, immediately refrigerated with ice
436 packs and frozen in common household freezers within 4 hours of collection. Samples were then
437 shipped frozen to Houston (USA) where they were stored at -80ºC until further analysis.

438 **Bottle corrosion testing with original produced water**

439 Production fluids (oil with associated water and gas) were collected at a pipeline outlet [I]
440 in a large oil field offshore Nigeria in December 2014. The fluids were filled into an internally
441 PTFE-lined steel drum (approx. 20 L) all the way to the brim and capped gas-tight. In the
442 laboratory, the content of the gas-tight drum was purged with N_2-CO_2 (79:21) to remove any
443 biogenic H_2S that had formed in the drum during transit (8 weeks). Thereafter, anoxic and sterile
444 technique was used to transfer the gravity-separated produced water into 1 L glass bottles (600 mL
445 each; pH 6.6 – pH 6.7) with butyl rubber stoppers under a N_2-CO_2 (79:21) headspace. For sterile
446 incubations, the capped produced water bottles were autoclaved (anaerobically) at 121ºC for 20
447 minutes. Three sterilized carbon steel coupons (3 x 1.25 cm^2) in a coupon holder made of polyether
448 ether ketone (PEEK) were added to each incubation (see Lahme et al., 2019 for details). Bottles
449 were placed on rotary shakers (75 rpm) and incubated at 32ºC or 60ºC for 13 weeks.

450 In March 2016, a second batch of production fluids was collected at a location further
451 downstream from the same pipeline [I], shipped to the laboratory (transit time: 5 weeks) and

452 processed as described above. Here, bottles with anoxic produced water (pH 6.6) were amended
453 with 1 mM sodium sulfate (Na_2SO_4) and incubated at 32ºC for 6 weeks.

454 **Bottle corrosion testing with synthetic produced water medium**

455 To study microbial corrosion under more defined conditions, bottle tests with synthetic
456 produced water medium were set up. The medium was modeled after the Nigerian produced water
457 (collected in March 2016 referred to below as PW-2016) and contained (all Sigma-Aldrich,
458 reagent-grade chemical in RO-DI water): NaCl (15.31 g/L), $MgCl_2 \cdot 6H_2O$ (0.562 g/L), $CaCl_2 \cdot 2H_2O$
459 (0.434 g/L), KCl (0.121 g/L) and NaBr (0.064 g/L). Additionally, Na_2SO_4 (1.48 g/L) was added
460 to allow for microbial sulfidogenesis. The brine was aliquoted (600 mL) into 1 L glass bottles,
461 purged with N_2-CO_2 (79:21), sealed with butyl rubber stoppers and autoclaved. After cooling, 24
462 mL/L of a sterile 1M $NaHCO_3$ stock solution (equilibrated with pure CO_2) was added.
463 Subsequently, the brines were supplemented with thiamine, a vitamin mixture, riboflavin, vitamin
464 B_{12}, a trace element mixture, selenite and tungstate, potassium phosphate and ammonium chloride
465 from sterile stock solutions (1 ml/L each), prepared as described previously (52). For
466 organotrophic test conditions, the medium was further supplemented with sodium acetate
467 ($NaCH_3CO_2$; 0.996 g/L) and sodium propionate ($NaC_3H_5O_2$; 0.157 g/L). The pH of the synthetic
468 produced water medium ranged from pH 6.6 to pH 6.7. Sterile carbon steel coupons in PEEK
469 coupon holders were added as described above, bottles were inoculated with 0.5% (vol/vol) of the
470 original field produced water and then incubated on rotary shakers (75 rpm) at 32°C for 11 weeks.

471 **Kettle corrosion testing**

472 Customized corrosion kettles were used to simulate the influence of pipeline flow on CO_2
473 corrosion and MIC (Fig. 3A). These reactors contained inward-facing corrosion coupons that were

474 flush-mounted in an inert coupon holder cage (PEEK) and thus arranged around a central impeller
475 with Rushton blades. The rotational speed was set to 500 rpm to correspond to an average coupon
476 wall shear stress of 7 Pa (7 kg m^{-1} s^{-2}), which was deemed representative of pipeline conditions
477 based on multi-phase flow modeling previously performed at this field. The glass reactor
478 containing 1.5 L of test brine was sealed air-tight, with continuous purging of N_2-CO_2 (79:21;
479 equivalent to 3 psia CO_2) through a diffusor (250 mL/min) and a gas outlet with refrigerated
480 condenser tube to minimize loss of liquids via evaporation. Corrosion kettles were temperature-
481 controlled at 32ºC by means of a heating jacket with thermo-couple. Control of pH was achieved
482 through titration with 1 M HCl via syringe pumps coupled to on-line pH monitoring and a set point
483 of pH 6.6. All tests contained four carbon steel coupons (5 cm^2 each) and were operated for 7
484 weeks, unless otherwise stated.

485 Prior to test setup, corrosion kettles were rigorously cleaned and then "de-contaminated"
486 through liberal application of acetone. Sterile test conditions cannot be achieved in corrosion
487 kettles. To minimize the growth of environmental contaminants, abiotic corrosion tests were
488 amended with the antibiotics kanamycin (100 mg/L), chloramphenicol (25 mg/L) and tetracycline
489 (20 mg/L), which did not affect acid gas corrosion rate or morphology in 7-day tests (Fig. S6).
490 Furthermore, vitamins, trace elements, phosphate and ammonium were omitted from abiotic
491 corrosion tests.

492 Corrosion testing was initially performed with the original PW-2016. This test included
493 1% (vol/vol) crude oil, was amended with sodium sulfate (10.4 mM; Na_2SO_4) and spiked with an
494 Fe^0-containing, sulfate-amended PW pre-enrichment as additional inoculum (3% vol/vol). Testing
495 under lithoautotrophic conditions was performed in synthetic produced water medium (no acetate,
496 propionate, or oil), inoculated with the first passage of a lithoautotrophic enrichment culture (0.5%

497 vol/vol) obtained from PW-2016. Finally, kettle corrosion testing was also performed with
498 synthetic produced water medium containing sodium acetate and sodium propionate as organic
499 electron donors for microbial metabolism and growth. This test was inoculated with the third
500 subculture of an organotrophic, Fe^0-containing enrichment (0.5% vol/vol) obtained from PW-
501 2016.

502 **Gas chromatography**

503 Methane in gaseous samples (10 mL) was quantified using an Agilent 490 Micro gas
504 chromatograph with thermal conductivity detector. Chromatography was performed on a heated
505 Agilent PoraPlot U column (50°C, 22.1 psi, 10 m), using argon as the carrier gas. Injector and
506 sample line temperature were set to 100°C.

507 **Weight loss corrosion analysis**

508 API 5L X52 carbon steel coupons (≤ 0.26% C, ≤ 0.45% Si, ≤ 1.6% Mn, < 0.03% P, ≤
509 0.03% S, balance Fe) were successively sonicated in hexane, acetone and methanol (5 min each),
510 dried in a stream of air and placed under vacuum overnight. The weight of each coupon was
511 measured three times on an analytical balance before placing into PEEK coupon holders. Coupon
512 holders containing corrosion coupons were sterilized by soaking in ethanol (96%) for 10 minutes.
513 Excess ethanol was dried with a stream of filtered N_2 gas.

514 At test end, corrosion products and other deposits were dissolved from coupons in a warm
515 (70°C) 1.8 N HCl solution containing 2% propargyl alcohol (1 min). Wet coupons were then
516 neutralized in saturated calcium hydroxide solution (30 sec) and scrubbed with a nylon brush while
517 being rinsed with deionized water. This procedure was performed twice. Coupons were then rinsed
518 in acetone, dried under a stream of air and placed under vacuum overnight. To determine weight

519 loss, each coupon was weighed three times. Corrosion rates were calculated by considering the
520 weight loss, exposed surface area, steel density (7.87 g/cm^3) and exposure time.

521 **Localized corrosion analysis**

522 To visualize and measure localized corrosion, the topography of cleaned carbon steel
523 coupons was mapped with a Keyence VR-3000K Wide-Area 3D profile measuring macroscope
524 (Keyence Corp., Itasca, IL). Corrosion features (≥ 25 μm in depth) were quantified by referencing
525 the original (pre-corrosion) surface height. Pitting corrosion rates, expressed as millimeter per
526 year, were calculated by linear extrapolation.

527 **DNA sampling and extraction**

528 Coupon holders were removed from bioreactors (bottles or corrosion kettles) and
529 thoroughly rinsed with sterile phosphate buffered saline (PBS) solution to remove loose
530 (planktonic) microorganisms. Steel-attached biofilms were then sampled using sterile swabs
531 (minimum of two swabs per coupon) and frozen at −80°C.

532 Frozen samples (pig debris or biofilm swabs) were shipped on ice to Microbial Insights
533 Inc. (Knoxville, TN) and DNA was extracted with the DNA Power Soil Total DNA Isolation kits
534 (MO BIO Laboratories, Inc., Solana Beach, CA) according to manufacturer's instructions. DNA
535 quantity and purity were assessed with a NanoDrop® ND-1000 spectrometer (Thermo Fisher
536 Scientific, Waltham, MA).

537 **Quantitative polymerase chain reaction**

538 Quantitative PCR was performed on a QuantStudio™ 12K Flex Real-Time PCR System
539 using a Taqman™ Universal PCR Mastermix (Applied Biosystems, Grand Island, NY). For the
540 quantification of eubacteria and archaea, primers and Taqman™ probes that target highly conserved

541 regions of the 16S rRNA gene were used as described elsewhere (53, 54). Forward and reverse
542 primers were obtained from Integrated DNA Technologies (Corralville, IA), while Taqman™
543 probes were synthesized by Thermo Fisher Scientific.

544 For the qPCR assay targeting the large subunit of the specific [NiFe] hydrogenase (here
545 referred to as *micH*) found in highly corrosive methanogenic archaea ((24) and this study), a
546 degenerated primer pair and Taqman™ probe were designed based on conserved regions in
547 homologous genes (Table 1, Fig. S7). Appropriate primer pairs and probes were selected using the
548 Primer Express™ software (Thermo Fisher Scientific) and initial specificity was assessed by
549 BLASTN searches against NCBI's nucleotide database (55). The qPCR reaction was performed
550 in 20 µl using the Taqman™ Universal PCR Mastermix. Forward and reverse primers, as well as
551 the probe were adjusted to a final concentration of 300 nM. For calibration and as positive control
552 a synthetic fragment of the *micH* gene was used (Fig. S7 and S8). The qPCR reaction conditions
553 were as follows: one cycle of 2 min at 50°C, followed by one cycle of 10 min at 95°C, 40 cycles
554 of 15 s at 95°C and 1 min at 60°C. The specificity of the qPCR reaction was verified by PCR melt
555 curve analysis and Sanger sequencing of final PCR products. In addition, potential cross reactions
556 were excluded by running the newly developed qPCR assay on genome-sequenced cultures (Table
557 S2) that lack the special [NiFe] hydrogenase (*micH*).

558 **16S rDNA amplicon sequencing and analysis**

559 16S rDNA amplicon sequencing was performed by GENEWIZ Inc. (South Plainfield, NJ).
560 DNA quality was assessed by agarose gel electrophoresis and quantified on a Qubit 2.0
561 Fluorometer (Invitrogen, Carlsbad, CA). Barcoded amplicons covering the V3 to V5 region of the
562 16S rRNA gene were generated using GENEWIZ's proprietary 16S MetaVx™ amplification
563 protocols and library preparation kit. Sequencing libraries were evaluated on an Agilent 2100

564 Bioanalyzer (Agilent Technologies, Palo Alto, CA) and quantified on a Qubit Fluorometer as well
565 as through qPCR. Paired-end sequencing (2× 250 bp) of multiplexed DNA libraries was performed
566 on an Illumina MiSeq platform (Illumina, San Diego, CA).

567 The 16S rRNA data was analyzed using the QIIME pipeline (56). Joined reads were quality
568 filtered, discarding reads with a mean quality score ≤ 20, a read length < 200 bp and reads
569 containing any ambiguous bases. Chimeric sequences were detected using the UCHIME algorithm
570 (https://drive5.com/uchime/uchime_download.html) and the Ribosomal Database Program (RDP)
571 Gold Database (57). After removal of chimeric sequences, the remainder of sequences was
572 assigned into operational taxonomic units (OTU) with the VSEARCH (v1.9.6) clustering program
573 and the SILVA 119 database (58), pre-clustered at 97% identity. Taxonomic categories were
574 assigned to all OTUs at a confidence threshold of 0.8 by the RDP classifier.

575 **Shotgun metagenome sequencing and analysis**

576 Shotgun sequencing of extracted DNA was performed by GENEWIZ Inc. The quality of
577 extracted DNA was assessed by agarose gel electrophoresis and quantified on a Qubit 2.0
578 Fluorometer. DNA libraries were prepared using the NEBNext® Ultra™ DNA Library Prep Kit
579 (New England BioLabs Inc., Ipswich, MA) according to manufacturer's instructions. Quality of
580 DNA libraries was evaluated using Agilent TapeStation and quantified using a Qubit Fluorometer.
581 Libraries were quantified by qPCR and then loaded on to an Illumina HiSeq 4000 platform
582 according to manufacturer's recommendations and sequenced using the paired-end (2× 150 bp)
583 configuration.

584 Subsequent bioinformatics analysis of paired-end sequencing reads was done in the KBase
585 environment (59). In summary, following quality trimming and adapter removal, the remaining

586 126 M paired-end reads were assembled with MetaSPAdes (v3.13.0) and a minimum contig size
587 of 500 bp (60). The assembled contigs were binned using the MetaBAT2 (v1.7) binning algorithm
588 (61). The quality of the resulting ten bins was evaluated using the CheckM (v1.0.18) software
589 package (62). Taxonomy was assigned to individual bins using the Genome Taxonomy Database
590 Toolkit (GTDB-Tk), which utilizes domain-specific, concatenated marker protein reference trees,
591 relative evolutionary divergence and average nucleotide identity for taxonomic classification (63).
592 Structural and functional annotation of binned contigs was achieved with NCBI's prokaryotic
593 annotation pipeline (64, 65). Additional annotations of unbinned contigs were obtained using the
594 Prokka software package (66).

595 **Data availability**

596 16S rRNA amplicon sequencing reads and shotgun metagenome reads used for assembly
597 and binning of individual genomes have been deposited to NCBI's sequencing reads archive and
598 the annotated draft genomes have been deposited at GenBank. The data can be accessed under the
599 bioproject PRJNA644413.

600 **ACKNOWLEDGEMENT**

601 We thank Manuel Castelan, Benny Chacko and Yao Xiong for their thoughtful discussions and
602 technical support throughout this project. We also greatly acknowledge the assistance provided by
603 Kingsley Oparaodu in obtaining several of the oil field samples.

604 **REFERENCES**

605 1. Migahed MA, Al-Sabagh AM. 2009. Beneficial role of surfactants as corrosion inhibitors in
606 petroleum industry: A review article. Chem Eng Commun 196:1054–1075.

607 2. Popoola LT, Grema AS, Latinwo GK, Gutti B, Balogun AS. 2013. Corrosion problems
608 during oil and gas production and its mitigation. Int J Ind Chem 4:35.

609 3. Nešić S. 2007. Key issues related to modelling of internal corrosion of oil and gas pipelines
610 – A review. Corros Sci 49:4308–4338.

611 4. Xiong Y, Fischer D, Cao F, Pacheco J. 2017. Impact of pre-corrosion on corrosion inhibitor
612 performance: Can we protect aged pipelines, paper NACE-2017-8919. NACE International,
613 NACE.

614 5. Xiong Y, Fischer D, Cao F, Pacheco J. 2019. Impact of steel metallurgy on corrosion inhibitor
615 performance: Another gap in industry practice, paper NACE-2019-12976. NACE
616 International, NACE.

617 6. Kip N, van Veen JA. 2015. The dual role of microbes in corrosion. The ISME Journal 9:542–
618 551.

619 7. Enning D, Garrelfs J. 2014. Corrosion of iron by sulfate-reducing bacteria: New views of an
620 old problem. Appl Environ Microbiol 80:1226–1236.

621 8. Enning D, Venzlaff H, Garrelfs J, Dinh HT, Meyer V, Mayrhofer K, Hassel AW, Stratmann
622 M, Widdel F. 2012. Marine sulfate-reducing bacteria cause serious corrosion of iron under
623 electroconductive biogenic mineral crust. Environ Microbiol 14:1772–1787.

624 9. Venzlaff H, Enning D, Srinivasan J, Mayrhofer KJJ, Hassel AW, Widdel F, Stratmann M.
625 2013. Accelerated cathodic reaction in microbial corrosion of iron due to direct electron
626 uptake by sulfate-reducing bacteria. Corros Sci 66:88–96.

627 10. Sharma M, Liu H, Chen S, Cheng F, Voordouw G, Gieg L. 2018. Effect of selected biocides
628 on microbiologically influenced corrosion caused by *Desulfovibrio ferrophilus* IS5. 1. Sci
629 Rep 8:16620.

630 11. Deng X, Dohmae N, Nealson KH, Hashimoto K, Okamoto A. 2018. Multi-heme cytochromes
631 provide a pathway for survival in energy-limited environments. Sci Adv 4:eaao5682.

632 12. Zhang T, Fang HHP, Ko BCB. 2003. Methanogen population in a marine biofilm corrosive
633 to mild steel. Appl Microbiol Biotechnol 63:101–106.

634 13. Dinh HT, Kuever J, Mußmann M, Hassel AW, Stratmann M, Widdel F. 2004. Iron corrosion
635 by novel anaerobic microorganisms. Nature 427:829–832.

636 14. Uchiyama T, Ito K, Mori K, Tsurumaru H, Harayama S. 2010. Iron-corroding methanogen
637 isolated from a crude-oil storage tank. Appl Environ Microbiol 76:1783–1788.

638 15. Usher KM, Kaksonen AH, MacLeod ID. 2014. Marine rust tubercles harbour iron corroding
639 archaea and sulphate reducing bacteria. Corros Sci 83:189–197.

640 16. Okoro C, Smith S, Chiejina L, Lumactud R, An D, Park HS, Voordouw J, Lomans BP,
641 Voordouw G. 2014. Comparison of microbial communities involved in souring and corrosion
642 in offshore and onshore oil production facilities in Nigeria. J Ind Microbiol Biotechnol
643 41:665–678.

644 17. Mand J, Park HS, Okoro C, Lomans BP, Smith S, Chiejina L, Voordouw G. 2016. Microbial
645 methane production associated with carbon steel corrosion in a Nigerian oil field. Front
646 Microbiol 6:1538.

647 18. Kip N, Jansen S, Leite MFA, de Hollander M, Afanasyev M, Kuramae EE, Veen JAV. 2017.
648 Methanogens predominate in natural corrosion protective layers on metal sheet piles. Sci Rep
649 7:11899.

650 19. Palacios PA, Snoeyenbos-West O, Löscher CR, Thamdrup B, Rotaru A-E. 2019. Baltic Sea
651 methanogens compete with acetogens for electrons from metallic iron. 12. ISME J 13:3011–
652 3023.

653 20. Daniels L, Belay N, Rajagopal BS, Weimer PJ. 1987. Bacterial methanogenesis and growth
654 from CO_2 with elemental iron as the sole source of electrons. Science 237:509–511.

655 21. Beese-Vasbender PF, Grote J-P, Garrelfs J, Stratmann M, Mayrhofer KJJ. 2015. Selective
656 microbial electrosynthesis of methane by a pure culture of a marine lithoautotrophic
657 archaeon. Bioelectrochemistry 102:50–55.

658 22. An BA, Kleinbub S, Ozcan O, Koerdt A. 2020. Iron to gas: Versatile multiport flow-column
659 revealed extremely high corrosion potential by methanogen-induced microbiologically
660 influenced corrosion (Mi-MIC). Front Microbiol 11:527.

661 23. Deutzmann JS, Sahin M, Spormann AM. 2015. Extracellular enzymes facilitate electron
662 uptake in biocorrosion and bioelectrosynthesis. mBio 6:e00496-15.

663 24. Tsurumaru H, Ito N, Mori K, Wakai S, Uchiyama T, Iino T, Hosoyama A, Ataku H, Nishijima
664 K, Mise M, Shimizu A, Harada T, Horikawa H, Ichikawa N, Sekigawa T, Jinno K, Tanikawa
665 S, Yamazaki J, Sasaki K, Yamazaki S, Fujita N, Harayama S. 2018. An extracellular [NiFe]
666 hydrogenase mediating iron corrosion is encoded in a genetically unstable genomic island in
667 *Methanococcus maripaludis*. Sci Rep 8:15149.

668 25. Skovhus TL, Eckert RB, Rodrigues E. 2017. Management and control of microbiologically
669 influenced corrosion (MIC) in the oil and gas industry—Overview and a North Sea case
670 study. J Biotechnol 256:31–45.

671 26. Kaye JZ, Márquez MC, Ventosa A, Baross JA. 2004. *Halomonas neptunia* sp. nov.,
672 *Halomonas sulfidaeris* sp. nov., *Halomonas axialensis* sp. nov. and *Halomonas*
673 *hydrothermalis* sp. nov.: halophilic bacteria isolated from deep-sea hydrothermal-vent
674 environments. Int J Syst Evol Microbiol 54:499–511.

675 27. Sousa DZ, Smidt H, Alves MM, Stams AJM. 2007. *Syntrophomonas zehnderi* sp. nov., an
676 anaerobe that degrades long-chain fatty acids in co-culture with *Methanobacterium*
677 *formicicum*. Int J Syst Evol Microbiol 57:609–615.

678 28. Nunoura T, Hirai M, Imachi H, Miyazaki M, Makita H, Hirayama H, Furushima Y,
679 Yamamoto H, Takai K. 2010. *Kosmotoga arenicorallina* sp. nov. a thermophilic and
680 obligately anaerobic heterotroph isolated from a shallow hydrothermal system occurring
681 within a coral reef, southern part of the Yaeyama Archipelago, Japan, reclassification of
682 *Thermococcoides shengliensis* as *Kosmotoga shengliensis* comb. nov., and emended
683 description of the genus *Kosmotoga*. Arch Microbiol 192:811–819.

684 29. Huber R, Woese CR, Langworthy TA, Kristjansson JK, Stetter KO. 1990. *Fervidobacterium*
685 *islandicum* sp. nov., a new extremely thermophilic eubacterium belonging to the
686 *Thermotogales*. Arch Microbiol 154:105–111.

687 30. Ravot G, Ollivier B, Magot M, Patel B, Crolet J, Fardeau M, Garcia J. 1995. Thiosulfate
688 reduction, an important physiological feature shared by members of the order *Thermotogales.*
689 Appl Environ Microbiol 61:2053–2055.

690 31. Miroshnichenko ML, Kostrikina NA, Chernyh NA, Pimenov NV, Tourova TP, Antipov AN,
691 Spring S, Stackebrandt E, Bonch-Osmolovskaya EA. 2003. *Caldithrix abyssi* gen. nov., sp.
692 nov., a nitrate-reducing, thermophilic, anaerobic bacterium isolated from a Mid-Atlantic
693 Ridge hydrothermal vent, represents a novel bacterial lineage. Int J Syst Evol Microbiol
694 53:323–329.

695 32. Waard C de, Lotz U, Dugstad A. 1995. Influence of liquid flow velocity on CO_2 corrosion:
696 A semi-empirical model. paper 106125, Corrosion ’95 conference, NACE International,
697 NACE.

698 33. Liu T, Cheng YF, Sharma M, Voordouw G. 2017. Effect of fluid flow on biofilm formation
699 and microbiologically influenced corrosion of pipelines in oilfield produced water. J Petrol
700 Sci Eng 156:451–459.

701 34. Duncan KE, Gieg LM, Parisi VA, Tanner RS, Tringe SG, Bristow J, Suflita JM. 2009.
702 Biocorrosive thermophilic microbial communities in Alaskan North Slope oil facilities.
703 Environ Sci Technol 43:7977–7984.

704 35. Vigneron A, Alsop EB, Chambers B, Lomans BP, Head IM, Tsesmetzis N. 2016.
705 Complementary microorganisms in highly corrosive biofilms from an offshore oil production
706 facility. Appl Environ Microbiol 82:2545–2554.

707 36. Mori K, Tsurumaru H, Harayama S. 2010. Iron corrosion activity of anaerobic hydrogen-
708 consuming microorganisms isolated from oil facilities. J Biosci Bioeng 110:426–430.

709 37. Bockris JO, Reddy AKN, Gamboa-Aldeco ME. 2000. Modern electrochemistry 2A:
710 Fundamentals of electrodics, Springer-Verlag, New York, NY

711 38. Kaesche H. 2003. Corrosion of metals: Physicochemical principles and current problems.
712 Springer-Verlag, Berlin Heidelberg.

713 39. Kahyarian A, Brown B, Nešić S. 2020. The unified mechanism of corrosion in aqueous weak
714 acids solutions: A review of the recent developments in mechanistic understandings of mild
715 steel corrosion in the presence of carboxylic acids, carbon dioxide, and hydrogen sulfide.
716 Corrosion 76:268–278.

717 40. von Wolzogen Kühr CAH, van der Vlugt LS. 1934. The graphitization of cast iron as an
718 electrobiochemical process in anaerobic soil. Water 18:147–165.

719 41. Starkey RL. 1947. Sulfate reduction and the anaerobic corrosion of iron. Antonie van
720 Leeuwenhoek 12:193–203.

721 42. Butlin KR, Adams ME, Thomas M. 1949. Sulphate-reducing bacteria and internal corrosion
722 of ferrous pipes conveying water. Nature 163:26–27.

723 43. Cord-Ruwisch R. 2000. Microbially influenced corrosion of steel, p. 159–173. *In* Loveley
724 DR (ed), Environmental microbe-metal interactions. ASM Press, Washington, DC.

725 44. Barker R, Burkle D, Charpentier T, Thompson H, Neville A. 2018. A review of iron carbonate
726 ($FeCO_3$) formation in the oil and gas industry. Corros Sci 142:312–341.

727 45. Deutzmann JS, Spormann AM. 2017. Enhanced microbial electrosynthesis by using defined
728 co-cultures. 3. ISME J 11:704–714.

729 46. Chen Y, Tang Q, Senko JM, Cheng G, Zhang Newby B, Castaneda H, Ju L-K. 2015. Long-
730 term survival of *Desulfovibrio vulgaris* on carbon steel and associated pitting corrosion.
731 Corros Sci 90:89–100.

732 47. Deng X, Dohmae N, Kaksonen AH, Okamoto A. 2020. Biogenic iron sulfide nanoparticles
733 to enable extracellular electron uptake in sulfate-reducing bacteria. Angew Chem Int Ed
734 132:6051–6055.

735 48. Krantz GP, Lucas K, Wunderlich EL-, Hoang LT, Avci R, Siuzdak G, Fields MW. 2019.
736 Bulk phase resource ratio alters carbon steel corrosion rates and endogenously produced
737 extracellular electron transfer mediators in a sulfate-reducing biofilm. Biofouling 35:669–
738 683.

739 49. Wikieł AJ, Datsenko I, Vera M, Sand W. 2014. Impact of *Desulfovibrio alaskensis* biofilms
740 on corrosion behaviour of carbon steel in marine environment. Bioelectrochemistry 97:52–
741 60.

742 50. Little BJ, Blackwood DJ, Hinks J, Lauro FM, Marsili E, Okamoto A, Rice SA, Wade SA,
743 Flemming H-C. 2020. Microbially influenced corrosion—Any progress? Corros Sci
744 170:108641.

745 51. Tejerizo GT, Kim YS, Maus I, Wibberg D, Winkler A, Off S, Pühler A, Scherer P, Schlüter
746 A. 2017. Genome sequence of *Methanobacterium congolense* strain Buetzberg, a

747 hydrogenotrophic, methanogenic archaeon, isolated from a mesophilic industrial-scale
748 biogas plant utilizing bio-waste. J Biotechnol 247:1–5.

749 52. Widdel F, Bak F. 1992. Gram-negative mesophilic sulfate-reducing bacteria, p. 3352–3378.
750 *In* Balows A, Truper HG, Dworkin M, Harder W, Schleifer K-H (ed), The prokaryotes, 2nd
751 ed, vol 4. Springer-Verlag, New York, NY.

752 53. Suzuki MT, Taylor LT, DeLong EF. 2000. Quantitative analysis of small-subunit rRNA
753 genes in mixed microbial populations via 5′-nuclease assays. Appl Environ Microbiol
754 66:4605–4614.

755 54. Yu Y, Lee C, Kim J, Hwang S. 2005. Group-specific primer and probe sets to detect
756 methanogenic communities using quantitative real-time polymerase chain reaction.
757 Biotechnol Bioeng 89:670–679.

758 55. Altschul SF, Gish W, Miller W, Myers EW, Lipman DJ. 1990. Basic local alignment search
759 tool. J Mol Biol 215:403–410.

760 56. Caporaso JG, Kuczynski J, Stombaugh J, Bittinger K, Bushman FD, Costello EK, Fierer N,
761 Peña AG, Goodrich JK, Gordon JI, Huttley GA, Kelley ST, Knights D, Koenig JE, Ley RE,
762 Lozupone CA, McDonald D, Muegge BD, Pirrung M, Reeder J, Sevinsky JR, Turnbaugh PJ,
763 Walters WA, Widmann J, Yatsunenko T, Zaneveld J, Knight R. 2010. QIIME allows analysis
764 of high-throughput community sequencing data. Nat Methods 7:335–336.

765 57. Cole JR, Wang Q, Fish JA, Chai B, McGarrell DM, Sun Y, Brown CT, Porras-Alfaro A,
766 Kuske CR, Tiedje JM. 2014. Ribosomal database project: data and tools for high throughput
767 rRNA analysis. Nucleic Acids Res 42:D633–D642.

768 58. Quast C, Pruesse E, Yilmaz P, Gerken J, Schweer T, Yarza P, Peplies J, Glöckner FO. 2013.
769 The SILVA ribosomal RNA gene database project: improved data processing and web-based
770 tools. Nucleic Acids Res 41:D590–D596.

771 59. Arkin AP, Cottingham RW, Henry CS, Harris NL, Stevens RL, Maslov S, Dehal P, Ware D,
772 Perez F, Canon S, Sneddon MW, Henderson ML, Riehl WJ, Murphy-Olson D, Chan SY,
773 Kamimura RT, Kumari S, Drake MM, Brettin TS, Glass EM, Chivian D, Gunter D, Weston
774 DJ, Allen BH, Baumohl J, Best AA, Bowen B, Brenner SE, Bun CC, Chandonia J-M, Chia
775 J-M, Colasanti R, Conrad N, Davis JJ, Davison BH, DeJongh M, Devoid S, Dietrich E,
776 Dubchak I, Edirisinghe JN, Fang G, Faria JP, Frybarger PM, Gerlach W, Gerstein M, Greiner
777 A, Gurtowski J, Haun HL, He F, Jain R, Joachimiak MP, Keegan KP, Kondo S, Kumar V,
778 Land ML, Meyer F, Mills M, Novichkov PS, Oh T, Olsen GJ, Olson R, Parrello B, Pasternak
779 S, Pearson E, Poon SS, Price GA, Ramakrishnan S, Ranjan P, Ronald PC, Schatz MC, Seaver
780 SMD, Shukla M, Sutormin RA, Syed MH, Thomason J, Tintle NL, Wang D, Xia F, Yoo H,
781 Yoo S, Yu D. 2018. KBase: The United States department of energy systems biology
782 knowledgebase. Nat Biotechnol 36:566–569.

783 60. Nurk S, Meleshko D, Korobeynikov A, Pevzner PA. 2017. metaSPAdes: a new versatile
784 metagenomic assembler. Genome Res 27:824–834.

785 61. Kang DD, Li F, Kirton E, Thomas A, Egan R, An H, Wang Z. 2019. MetaBAT 2: an adaptive
786 binning algorithm for robust and efficient genome reconstruction from metagenome
787 assemblies. PeerJ 7:e7359.

788 62. Parks DH, Imelfort M, Skennerton CT, Hugenholtz P, Tyson GW. 2015. CheckM: assessing
789 the quality of microbial genomes recovered from isolates, single cells, and metagenomes.
790 Genome Res 25:1043–1055.

791 63. Chaumeil P-A, Mussig AJ, Hugenholtz P, Parks DH. 2020. GTDB-Tk: a toolkit to classify
792 genomes with the Genome Taxonomy Database. Bioinformatics 36:1925–1927.

793 64. Tatusova T, DiCuccio M, Badretdin A, Chetvernin V, Nawrocki EP, Zaslavsky L, Lomsadze
794 A, Pruitt KD, Borodovsky M, Ostell J. 2016. NCBI prokaryotic genome annotation pipeline.
795 Nucleic Acids Res 44:6614–6624.

796 65. Haft DH, DiCuccio M, Badretdin A, Brover V, Chetvernin V, O'Neill K, Li W, Chitsaz F,
797 Derbyshire MK, Gonzales NR, Gwadz M, Lu F, Marchler GH, Song JS, Thanki N, Yamashita
798 RA, Zheng C, Thibaud-Nissen F, Geer LY, Marchler-Bauer A, Pruitt KD. 2018. RefSeq: an
799 update on prokaryotic genome annotation and curation. Nucleic Acids Res 46:D851–D860.

800 66. Seemann T. 2014. Prokka: rapid prokaryotic genome annotation. Bioinformatics 30:2068–
801 2069.

802 **TABLE AND FIGURE CAPTIONS**

803 **Table 1** Sequences of degenerate primer pair and probe used in qPCR assays to detect the
804 proposed methanogenic MIC biomarker *micH*.

805 **Table 2** Metagenome-assembled genomes (MAG) of methanogenic and sulfate-reducing
806 microorganisms in severely corrosive biofilm.

807 **Figure 1** Archaeal community composition in solid samples (pig debris) collected from carbon
808 steel pipelines. Archaeal sequences accounted for between 0.2% and 21.6% of all reads from 16S
809 rRNA gene sequencing of DNA extracted from pipeline solids (top row). Total 16S rRNA gene
810 numbers (archaeal + bacterial) and gene copy numbers of the proposed methanogenic MIC
811 biomarker *micH* are also plotted for each sample. Pipelines (A – H) are ordered according to their
812 perceived severity of MIC (increasing from left to right, as indicated by arrow). The perceived
813 (qualitative) severity of MIC is based on inspection data (in-line inspection, ILI), field and
814 laboratory studies, as well as operator experience. A: Offshore multi-phase pipeline (East Asia).
815 B: Offshore crude transmission pipeline (U.S. Gulf of Mexico). C: Offshore multi-phase pipeline
816 (U.S. West Coast). D: Onshore crude transmission pipeline (U.S. Gulf Cast). E: Onshore crude
817 transmission pipeline (U.S. West Coast). F: Onshore produced water pipeline (U.S. Midwest). G:
818 Offshore multi-phase pipeline (Nigeria). H: Offshore multi-phase pipeline (U.S. West Coast). I:
819 Offshore multi-phase pipeline (Nigeria).

820 **Figure 2** Growth of steel-attached oil field biofilms in bottle tests. A – C Tests with sulfate-free
821 anoxic produced water as obtained from the West African oil field and incubated under mesophilic
822 (32°C) and thermophilic (60°C) conditions. D – F Tests with sulfate-amended produced water, as
823 well as synthetic produced water media (+ sulfate) in the presence or absence of propionate and
824 acetate (organotrophic and lithotrophic conditions, respectively).). A and D Averaged weight loss
825 corrosion rates (CR), total 16S rRNA gene (archaeal + bacterial) quantification and gene copy
826 numbers of the proposed archaeal MIC biomarker *micH*. A threshold denoting technically relevant,
827 high corrosion rates ($\geq$ 0.13 mm Fe^0 yr^{-1}) is indicated by the dashed red line. Methane formation
828 is depicted as final concentration in headspace after 3 months (A). Archaeal (B and E) and bacterial
829 (C and F) community composition was assessed by 16S rRNA gene sequencing of DNA extracted

830 from biofilms grown on carbon steel coupons. Archaeal sequences account for 0.1 – 54.4% and
831 bacterial sequences for 40.3 – 99.8% of the total sequencing reads. The enrichment culture that
832 was used for a subsequent lithotrophic corrosion kettle test is indicted by an asterisk.

833 **Figure 3** Growth of steel-attached oil field biofilms in corrosion kettle tests. A) Schematic of
834 customized corrosion kettles for the study of CO_2 corrosion and MIC under pipeline-simulating
835 conditions (flow and acid-gas purging). B) Averaged weight loss corrosion rates (CR) in anoxic
836 kettle tests containing oil field microorganisms in West African produced water, as well as
837 synthetic produced water media with or without addition of the organic electron donors acetate
838 and propionate (organotrophic and lithotrophic conditions, respectively). A sterile control test
839 quantifying CO_2 corrosion was also included. Total 16S rRNA gene (archaeal + bacterial)
840 quantification and gene copy numbers of the proposed archaeal MIC biomarker *micH* in coupon
841 biofilms are plotted for each test. A threshold denoting technically relevant, high corrosion rates
842 ($\geq$ 0.13 mm Fe^0 yr^{-1}) is indicated by the dashed red line. False color images show the topography
843 of coupons at the end of the experiments after removal of corrosion products. The average maximal
844 feature depth from four steel coupons per test and corresponding linearly extrapolated pitting
845 corrosion rates are provided in the sub-panel. The asterisk indicates the test selected for
846 metagenomic analysis.

847 **Figure 4** Comparison of the genetic arrangement of the 'MIC island' in *Methanococcus*
848 *maripaludis* strain OS7 (MMOS7) and the metagenome-assembled genome (MIC098Bin5) of a
849 *M. maripaludis* strain grown on severely corroded steel surfaces. The scale bars indicate the
850 nucleotide position in the individual genomes.

Table 1 Sequences of degenerate primer pair and probe used in qPCR assays to detect the proposed methanogenic MIC biomarker *micH*.

Primer/Probe	Sequence (5' → 3')[a]	Product length (bp)
micH-fwd	AA(Y)CTTCTAACACCAA(M)TGA(Y)GGAAC	95
micH-rev	TCAAATCCTCTAAATTCTGTGACACA	
micH-probe	TACCAACAGATAATGCTGCA	

[a] M = A or C; Y = C or T

Table 2 Metagenome-assembled genomes (MAG) of methanogenic and sulfate-reducing microorganisms in severely corrosive biofilm.

Taxonomic assignment [a]	Total sequence length (bp)	No. Contigs	N50	L50	Completeness [b]	Contamination [b]
Methanococcus maripaludis	1,702,487	5	989,172	1	99.5%	0.5
Desulfovibrio alaskensis	3,270,933	67	84,479	12	99.4%	0.0
Desulfovibrionaceae	3,278,183	87	63,483	16	99.4%	0.0
Desulfovibrionaceae	4,247,882	120	82,594	15	99.4%	0.0

[a] Taxonomic assignment is based on GTDB-Tk classification; [b] Completeness and contamination was estimated using CheckM

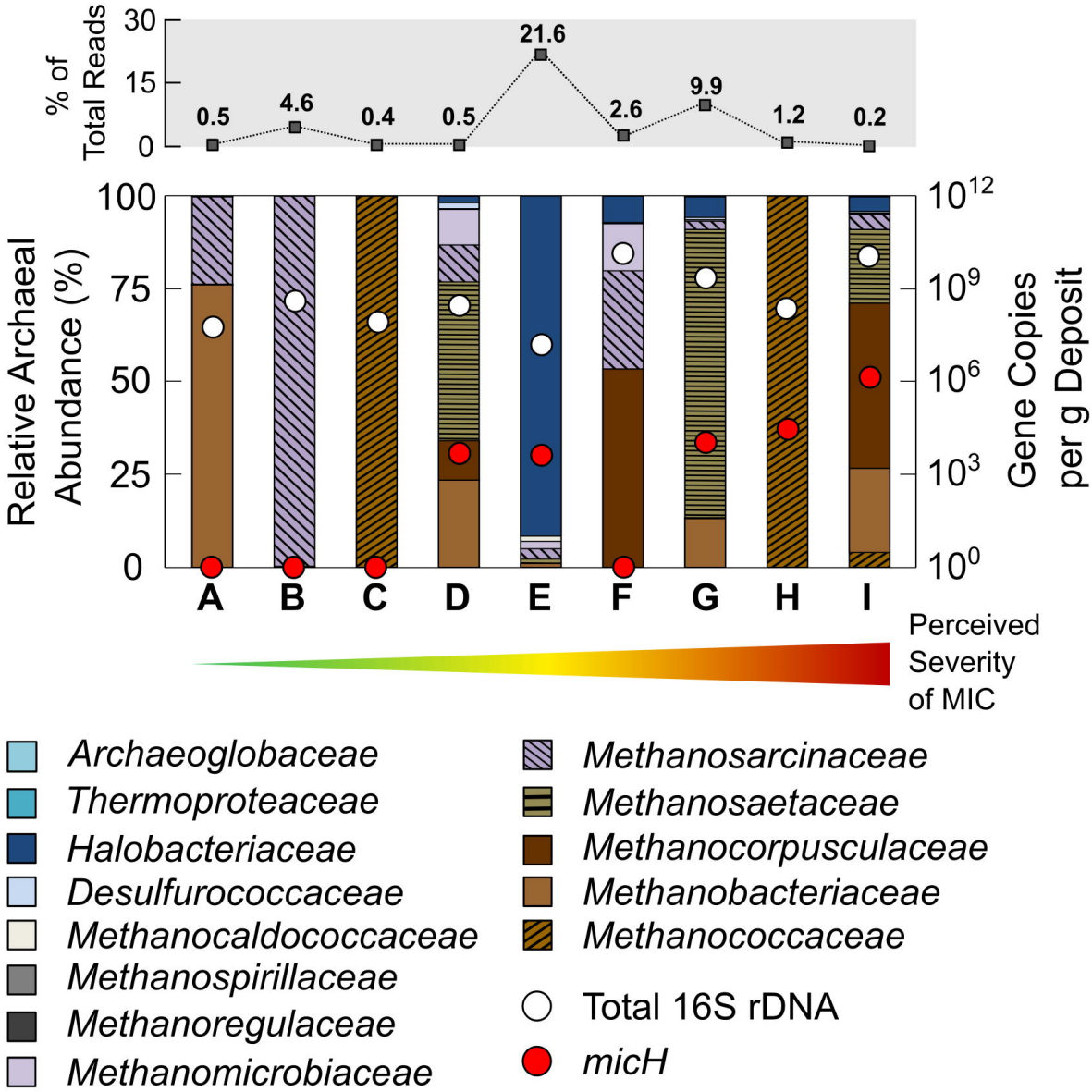

Figure 1 Archaeal community composition in solid samples (pig debris) collected from carbon steel pipelines. Archaeal sequences accounted for between 0.2% and 21.6% of all reads from 16S rRNA gene sequencing of DNA extracted from pipeline solids (top row). Total 16S rRNA gene numbers (archaeal + bacterial) and gene copy numbers of the proposed methanogenic MIC biomarker *micH* are also plotted for each sample. Pipelines (A – H) are ordered according to their perceived severity of MIC (increasing from left to right, as indicated by arrow). The perceived (qualitative) severity of MIC is based on inspection data (in-line inspection, ILI), field and laboratory studies, as well as operator experience. A: Offshore multi-phase pipeline (East Asia). B: Offshore crude transmission pipeline (U.S. Gulf of Mexico). C: Offshore multi-phase pipeline (U.S. West Coast). D: Onshore crude transmission pipeline (U.S. Gulf Cast). E: Onshore crude transmission pipeline (U.S. West Coast). F: Onshore produced water pipeline (U.S. Midwest). G: Offshore multi-phase pipeline (Nigeria). H: Offshore multi-phase pipeline (U.S. West Coast). I: Offshore multi-phase pipeline (Nigeria).

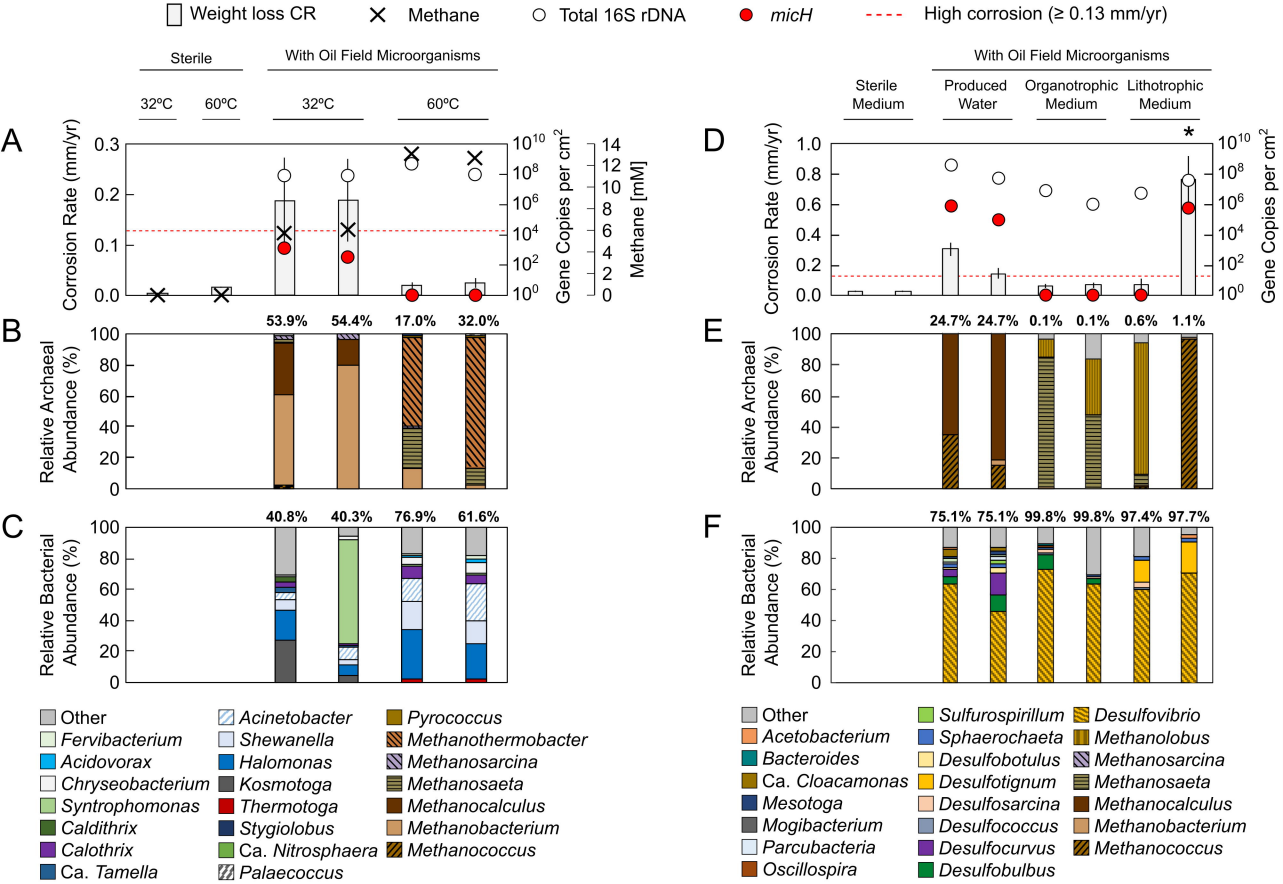

Figure 2 Growth of steel-attached oil field biofilms in bottle tests. A – C Tests with sulfate-free anoxic produced water as obtained from the West African oil field and incubated under mesophilic (32°C) and thermophilic (60°C) conditions. D – F Tests with sulfate-amended produced water, as well as synthetic produced water media (+ sulfate) in the presence or absence of propionate and acetate (organotrophic and lithotrophic conditions, respectively).). A and D Averaged weight loss corrosion rates (CR), total 16S rRNA gene (archaeal + bacterial) quantification and gene copy numbers of the proposed archaeal MIC biomarker *micH*. A threshold denoting technically relevant, high corrosion rates (≥ 0.13 mm Fe0 yr-1) is indicated by the dashed red line. Methane formation is depicted as final concentration in headspace after 3 months (A). Archaeal (B and E) and bacterial (C and F) community composition was assessed by 16S rRNA gene sequencing of DNA extracted from biofilms grown on carbon steel coupons. Archaeal sequences account for 0.1 – 54.4% and bacterial sequences for 40.3 – 99.8% of the total sequencing reads. The enrichment culture that was used for a subsequent lithotrophic corrosion kettle test is indicted by an asterisk.

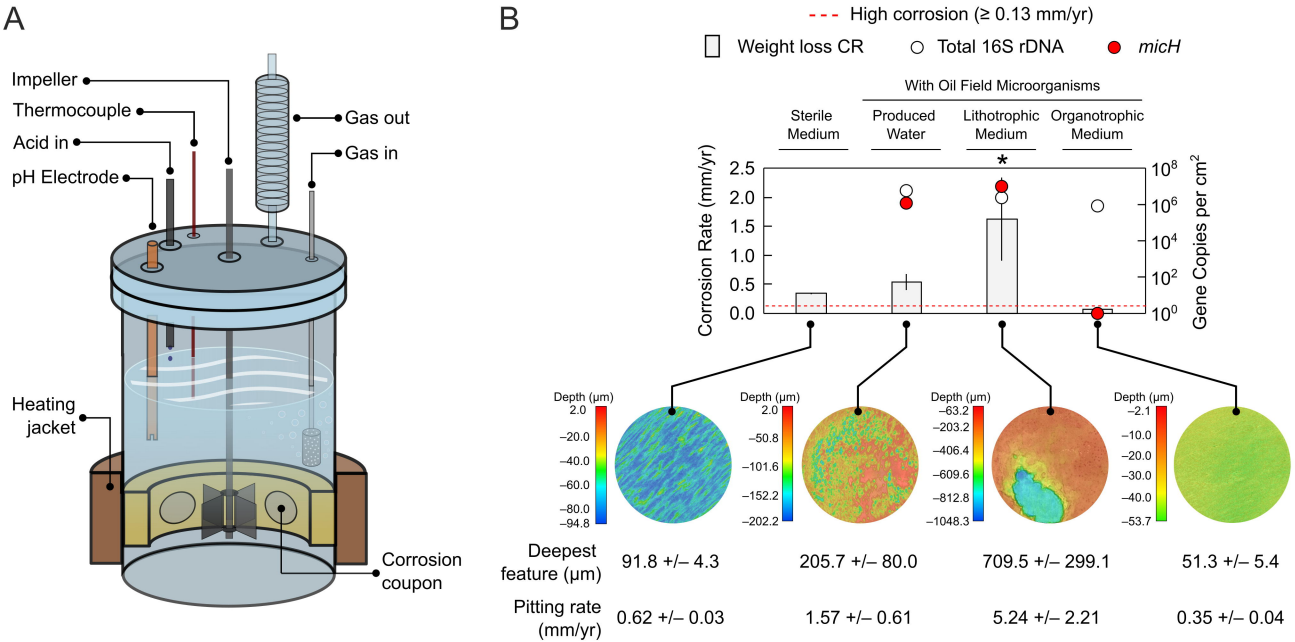

Figure 3 Growth of steel-attached oil field biofilms in corrosion kettle tests. A) Schematic of customized corrosion kettles for the study of CO_2 corrosion and MIC under pipeline-simulating conditions (flow and acid-gas purging). B) Averaged weight loss corrosion rates (CR) in anoxic kettle tests containing oil field microorganisms in West African produced water, as well as synthetic produced water media with or without addition of the organic electron donors acetate and propionate (organotrophic and lithotrophic conditions, respectively). A sterile control test quantifying CO_2 corrosion was also included. Total 16S rRNA gene (archaeal + bacterial) quantification and gene copy numbers of the proposed archaeal MIC biomarker *micH* in coupon biofilms are plotted for each test. A threshold denoting technically relevant, high corrosion rates (≥ 0.13 mm Fe^0 yr^{-1}) is indicated by the dashed red line. False color images show the topography of coupons at the end of the experiments after removal of corrosion products. The average maximal feature depth from four steel coupons per test and corresponding linearly extrapolated pitting corrosion rates are provided in the sub-panel. The asterisk indicates the test selected for metagenomic analysis.

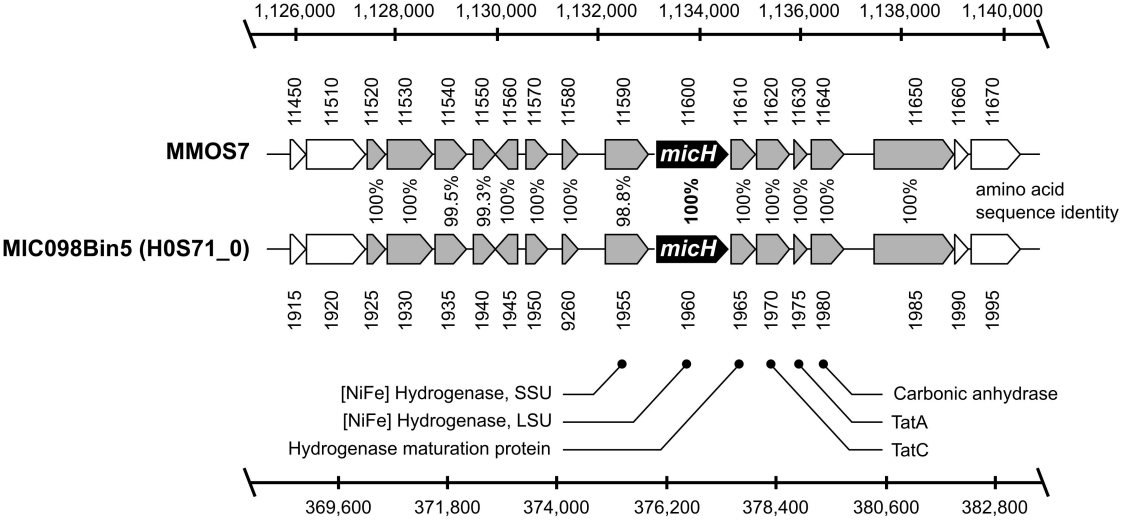

Figure 4 Comparison of the genetic arrangement of the 'MIC island' in *Methanococcus maripaludis* strain OS7 (MMOS7) and the metagenome-assembled genome (MIC098Bin5) of a *M. maripaludis* strain grown on severely corroded steel surfaces. The scale bars indicate the nucleotide position in the individual genomes.